

# Performance of Assessment Tool for Preoperative Planning of Brain Tumor Resection

<sup>1</sup>Dr. V. K. Narendira Kumar, <sup>2</sup>G. Prabhu, <sup>3</sup>N. Geetha, <sup>4</sup>R. Santhosh

<sup>1,4</sup>Assistant Professor of Computer Science, <sup>2,3</sup>Assistant Professors of Information Technology,  
Gobi Arts & Science College (Autonomous), Gobichettipalayam, Erode District, Tamil Nadu, India.

## ABSTRACT

A patient precise finite constituent biphasic brain model has been making use of to codify a surgeon's experience by establishing quantifiable biomechanical measures to achieve orientations for optimal preparation of brain tumor resection. When faced by means of evaluating more than a few potential approaches to tumor removal during preoperative planning, the objective of this exertion is to make easy the surgeon's selection of a patient head orientation such that tumor presentation and resection is help by means of positive brain shift conditions rather than trying to allay confounding ones. Displacement-based procedures consisting of region classification of the brain surface shifting in the craniotomy region and lateral displacement of the tumor center relative to an approach vector distinct by the surgeon were calculated over a variety of orientations and second-hand to form an objective function. For a frontal lobe tumor presentation, the reproduction predicts an perfect orientation that point to s the patient should be positioned in a on the side deceits place on the side contra lateral to the tumor in arrange to minimize unfavorable brain shift.

**Keywords :** Brain Shift, Patient Positioning, Tumor Resection, Finite Elements.

## I. INTRODUCTION

Neurological procedures involving the resection of brain tumors require the surgeon to evaluate the most desirable approach for extraction, one which facilitates tumor access and removal while minimizing damage to surrounding healthy tissue. Intraoperative brain shift complicates this evaluation. Studies in the literature have reported non-rigid deformation of a centimeter or more[1] during surgery owing to a variety of reasons such as administration of hyperosmotic drugs, edema, gravity, pathology, respiration, and surgical manipulation.[2,3,4] The shift causes concerns with the conformance of the visual presentation of the brain to the preoperative tomograms being used for

image guidance. This compromise of the spatial relationship between physical space in the operating room (OR) and the patient's preoperative image tomograms in the context of image-guided surgery suggests that an evaluation tool for minimizing shift might be used to reduce the discrepancy between the two.

Besides issues with image guidance, brain shift also frequently requires the usage of retractors to obtain favorable access to the tumor. The resultant retraction forces potentially damage healthy tissue. To mitigate the possible consequences of applying retraction, one possible approach is to orient the patient to where gravity and other shift mechanisms generate a favorable brain shift such that the use of retraction is minimized. Towards this end, analysis of

the underlying patient positioning criteria used by our participating surgeon has suggested a series of biomechanical measures that form a basis upon which to optimize model-based selection of patient orientation in the following work.

In previous work V.K. Narendira Kumar et al [17] demonstrated increased mid-line tumor accessibility for tumors in close proximity to the falx cerebri based upon tumor stress criteria. The position-dependent gravitationally induced tensile stresses on the tumor surface pulling the surrounding brain tissue away from the tumor was found to allow easier resection and reduced likelihood for the need for retraction.

However, this enhanced tumor exposure was noted to come at the expense of greater intraoperative shift. The following work examines a large frontal lobe tumor in the context of shift minimization to demonstrate a possible solution to the nontrivial task of patient positioning for surgery [5].

## II. BRAIN TUMORS

A brain tumor is an intracranial mass produced by an uncontrolled growth of cells either normally found in the brain such as neurons, lymphatic tissue, glial cells, blood vessels, pituitary and pineal gland, skull, or spread from cancers primarily located in other organs [2].

Brain tumors are classified based on the type of tissue involved, the location of the tumor, whether it is benign or malignant, and other considerations. Primary (true) brain tumors are the tumors that originated in the brain and are named for the cell types from which they originated. They can be benign (non cancerous), meaning that they do not spread elsewhere or invade surrounding tissues. They can also be malignant and invasive (spreading to neighboring area). Secondary or metastasis brain tumors take their origin from tumor cells which spread to the brain from another location in the body. Most often cancers that spread to the brain to cause secondary brain tumors originate in the lung, breast,

and kidney or from melanomas in the skin by V.K. Narendira Kumar et al.

Each primary brain tumor, in addition to the solid portion of the tumor, may have other associated parts such as edema and necrosis as in Figures 2 and 3. Edema is one of the most important factors leading to mortality associated with brain tumors. By definition, brain edema is an increase in brain volume resulting from increased sodium and water content and results from local disruption of the Blood Brain Barrier (BBB).

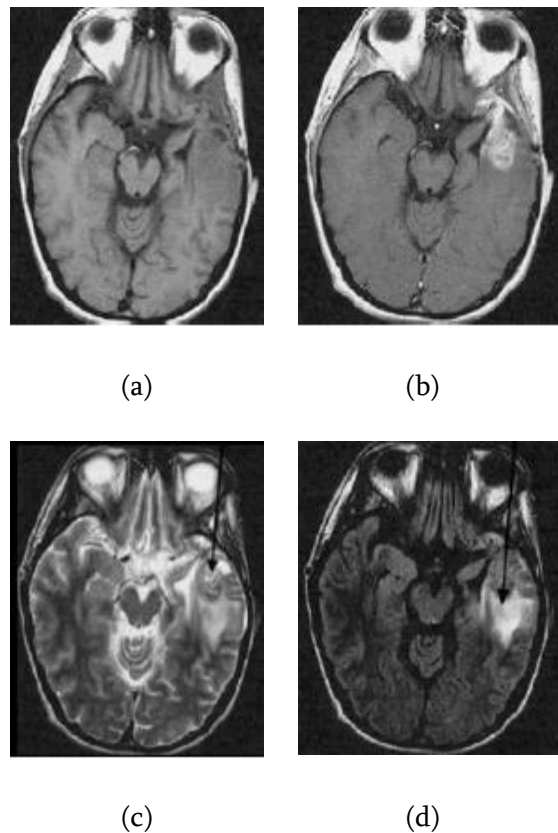


**Figure 2 :** MRI of brain. (a) T1-weighted image without contrast enhancement. (b) T1-weighted image with contrast enhancement. (c) T2-weighted image. (d) FLAIR image.

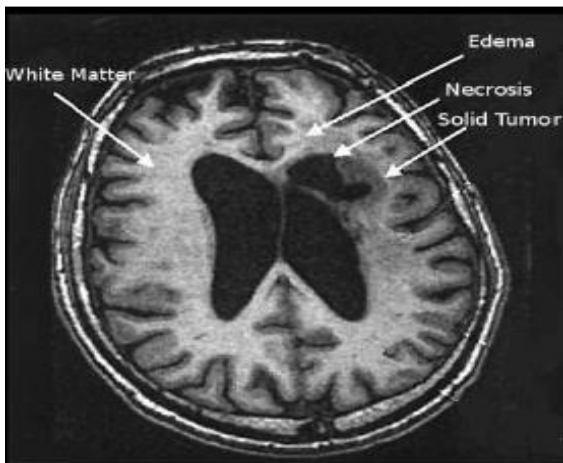


**Figure 3 :** One axial slice of a MR image of the brain showing tumor areas.

Edema appears around the tumor mainly in white matter regions. Tumor associated edema is visible in MRI, as either hypo intense (darker than brain tissue) or rarely is intense (same intensity as brain tissue) in T1-weighted scans, or hyper intense (brighter than brain tissue) in T2-weighted and FLAIR MRI (Figure 3). Necrosis is composed of dead cells in the middle of the brain tumor and is seen hypo intense in T1-weighted images (Figure 3). A brain tumor may also infiltrate the surrounding tissues or deform the surrounding structures by V.K. Narendira Kumar et al [19].

### A. Classification of Brain Tumors

The classification of primary brain tumors is usually based on the tissue of origin, and occasionally on tumor location. The degree of tumor malignancy is determined by the tumor's histopathology features. Because of the substantial variety and unusual biology of brain tumors, it has been extremely difficult to develop a widely accepted histological classification system [4].

The earliest brain tumor classifications were provided by Bailey and Cushing in 1926. Their classification scheme proposed 14 brain tumor types, directed important attention to the process of cell differentiation, and dominated views of gliomas until 1949 when a new system was introduced by Kernohan and Sayre. Kernohan and Sayre made the important realization that different histopathology

appearances may not represent separate tumor types but rather different degrees of differentiation of one tumor type. They classified tumors into five subtypes: astrocytoma, oligodendroglioma, ependymoma, gangliocytoma, and medulloblastoma and very importantly added a four-level grading system for astrocytomas [1]. The grading system was based on increasing malignancy and decreasing differentiation with increasing tumor grade. The addition of a grading system was a very important advance in classifying brain tumors, and provided information not only regarding tumors' biologic behavior but also information that could be used to guide treatment decisions.

### B. Brain Tumor Segmentation

Despite numerous efforts and promising results in the medical imaging community, accurate and reproducible segmentation and characterization of abnormalities are still a challenging and difficult task because of the variety of the possible shapes, locations and image intensities of various types of tumors. Some of them may also deform the surrounding structures or may be associated to edema or necrosis that changes the image intensity around the tumor. As we surveyed in the previous chapter, existing methods leave significant room for increased automation, applicability and accuracy. Most of them are usually dedicated to full-enhanced tumors or specific types of tumors, and do not extent easily to more general types [5].

The automated brain tumor segmentation method that we have developed consists of two main components: preprocessing and segmentation. The inputs of this system are two different modalities of MR images: CE-T1w and FLAIR that we believe are sufficient for brain tumor segmentation [2]. In the segmentation preprocessing section, operations such as: reduction of intensity inhomogeneity and inter-slice intensity variation of images, spatial registration (alignment) of the input images, segmentation of the brain, computation of the approximate symmetry

plane and histogram analysis based on symmetry plane are performed.

### III. PREPROCESSING

In the real MRI data there are some problems that have to be first solved before any segmentation operation. Therefore we first try to reduce the intensity in homogeneity and inter slice intensity variations, two main problems of MRI data, in the input images. Our system uses two different modalities of MRI, usually not spatially aligned and often having different resolutions. Hence it is required to add a registration and interpolation step. The brain is then segmented by a combination of histogram analysis, morphological operations and symmetry analysis. In this step we compute the approximate symmetry plane that will be used in the segmentation and sometimes to correct the brain segmentation result. Finally we analyze the histograms of the right and left hemispheres to detect the pathological hemisphere and the type of tumor.

#### A. Image Preprocessing

Two main problems of MR images are intensity inhomogeneity or bias field and interslice intensity variations which are caused by the limitations of the current MRI equipments (the main factors are RF excitation field inhomogeneity, non-uniform reception coil sensitivity, eddy currents driven by field gradients, RF penetration and standing wave effects).

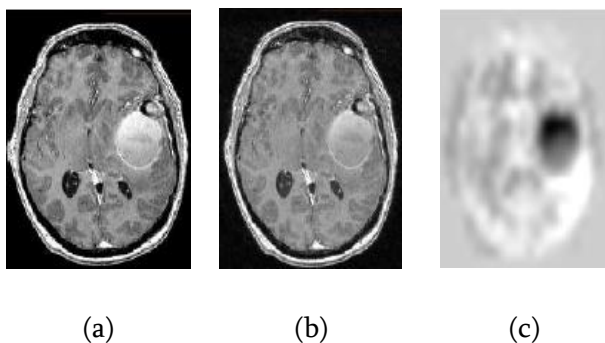


**Figure 4 :** Bias field correction. (a) An axial slice of the original image. (b) Same bias field corrected slice. (c) Applied bias field.

In today MR images, the bias field is not always visible to the human observer, but it causes significant tissue misclassification problems when intensity-based segmentation is used [7]. Therefore, it is required to correct intensity inhomogeneity in the image volume.

An automatic method based on entropy minimization is used (as seen in Figure 4). In addition to a smoothly varying field inhomogeneity, two-dimensional multislice sequence MR images, which are acquired in an interleaved way, are typically also corrupted with a slice by slice constant intensity offset. This is usually due to gradient eddy currents and crosstalk between slices. Hence, it is required to normalize interslice intensity to have a correct 3D segmentation. Here a method based on scale-space analysis of histogram is used [9].

#### B. Image Registration

Image registration is the operation of aligning images in order to relate corresponding features. For most kinds of image processing on two or more images, it is required that the images are aligned, so that one voxel position represents the same anatomical position in all images [10]. This step allows the use of modalities that are not in perfect alignment. An image registration program has typically four modules: the transformation model, feature extraction, similarity measure, and an optimization method. In our system, the CE-T1w image is used as reference or target image (R) and the FLAIR image as test or source image (T).

Several transformation models can be used to transform the test image T, such as rigid, affine, projection and curved transformations. Here, the registration concerns 3D head images from the same person, which makes it reasonable to assume that the head will not be deformed, and thus can be considered a rigid body. Hence, the rigid transformation model (rotation and translation) is therefore sufficient for our purpose. By using a rigid transformation, we are assuming that the two images can be aligned using a parameterization with 6

degrees of freedom. Here we restrict ourselves to methods that use directly the intensity images as features, thus avoiding the preliminary extraction of corresponding features in the two images.

### C. Brain Segmentation

The next step of preprocessing consists of brain segmentation. Several methods have been proposed to perform this operation and some of them are available in software's such as Brain-Visa, FSL and Brain suite. Unfortunately most of them fail in the case of the presence of a tumor in the brain, especially if located on the border of the brain (Figure 5).

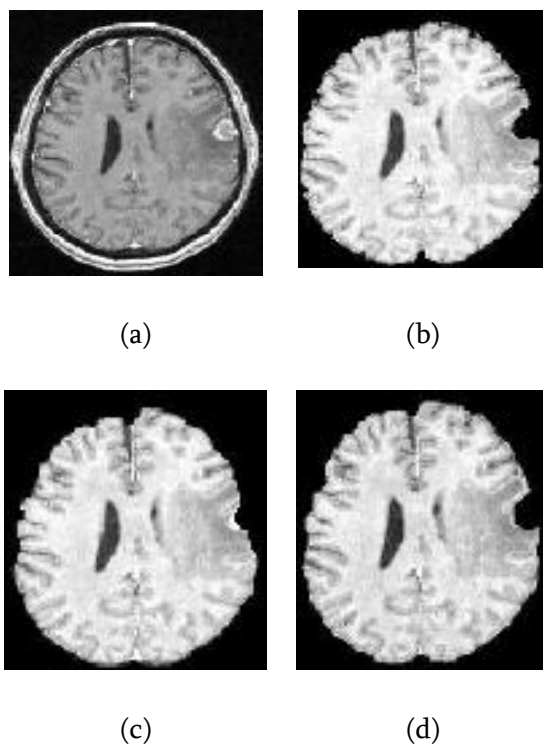


**Figure 5** : Pathological brain segmentation using existing methods. (a) One slice of the original image on two examples. (b) Segmented brain by histogram analysis and morphological operations using Brain Visa. (c) Segmented brain by BET using FSL. (d) Segmented brain by BSE using Brain suite.

To solve this problem, we propose to perform a symmetry analysis, based on the assumption that tumors are generally not symmetrically placed in both hemispheres, while the whole brain is approximately symmetrical. First we segment the brain using histogram analysis and morphological

operations. This leads to a partial segmentation, where a part corresponding to the tumor may be missing. The algorithm is applied on the gray level image of the head to compute the approximate symmetry plane, because the segmented brain is not symmetric. The computed symmetry planes of the head and of the segmented brain in normal cases are approximately equal and this approximation is acceptable in pathological cases for tumor detection purpose.

### D. Structure Segmentation

The proposed method for internal brain structures segmentation, such as for tumors, has two phases: initialization and refinement. In other words, we first segment the brain tissues (consequently the internal structures of the brain) and since this segmentation for internal brain structures is not fine enough, we then refine them one by one using prior information. To perform these two phases, the segmentation procedure consists of the following steps [6]:

- Global segmentation of the brain,
- Retrieving spatial relations,
- Selecting the valid spatial relations,
- Fuzzification and fusion of relations and providing the ROI,
- Searching the initial segmentation of structure,
- Refining the initial segmentation,
- Repeating from step 2 for other structures.

Global segmentation of the brain to segment the brain tissues and its structures we use two methods, the first one is the MPFCM method and the second one is the multiphase level sets.

## IV. SYSTEM METHODS

A 3D finite element computational brain model based upon Biot's theory of soil consolidation [8] was used to simulate brain shift under varying conditions. Biot's consolidation theory describes the mechanical behavior of a poroelastic medium<sup>1</sup> using a linearly elastic description of the solid matrix and Darcy's law for fluid flow through the porous matrix.

Deformations can be caused by surface forces, displacements, interstitial fluid pressure gradients, or changes to tissue buoyancy. Changes in the volumetric strain rate depend upon the interstitial pressure and hydration. The usage of this biphasic model for simulating the soft tissue mechanics associated with brain shift is well established in the literature.[4,6,7,9,10,11,12,13] This particular model has been previously validated for performing model-updated image guided surgery in phantom, animal, and human studies.[4,6,7,9,10,11]

### **A. Model and Boundary Condition Generation**

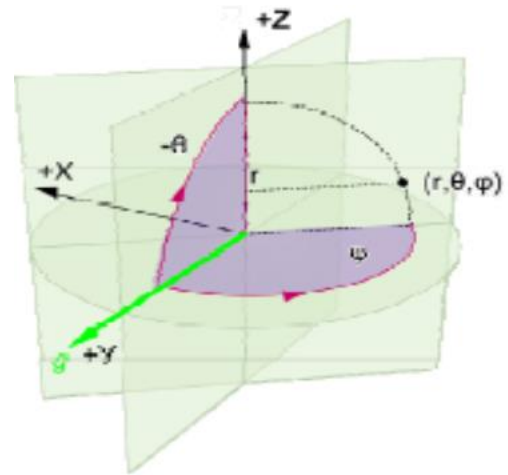
Observation within the OR of the surgical planning phase suggests that the surgeon defines an 'approach' vector to the tumor via use of an image-guidance system. This vector is the line that extends from the center of the tumor to a point on the scalp the surgeon notes the tumor lies directly under with a guidance probe. Upon exposure of the skull, this point is again marked, indicating it is a significant landmark, and typically lies in the center of the chosen craniotomy. This important vector is used within this work for resection of the brain mesh and for determining the quantitative measures. For the clinical case being analyzed, it was approximated as the normal to the craniotomy region created by averaging all the node normals within the craniotomy by V.K. Narendira Kumar et al [18].

Generation of a patient-specific brain model utilizes pre-surgical planning and data realized by the surgeon. The brain and tumor surfaces are first segmented manually from a gadolinium-enhanced tomographic image volume. A tetrahedral mesh of approximately 120,000 elements is then created using these surfaces and the material types of the mesh elements are classified as gray or white matter according to gray scale thresholds applied to the image volume via an image-to-grid method.[15,16] The brain surface surrounding the craniotomy and the tumor surface are refined such that the characteristic length of a boundary element is half that elsewhere.

A patient specific falx cerebri membrane is inserted by splitting the mesh and applying special boundary conditions-- no displacement across the falx but the brain and falx are allowed to slip along the cranial wall. The elements classified as tumor are removed via a resection element list which decouples the respective equilibrium equation. Additionally, a cylindrical plug of tissue from tumor center to brain surface with axis being the 'approach' vector and of radius 70% of the average tumor radius is removed from the mesh to allow relaxation into the resultant resection cavity. All elements with centroid coordinates within the radius as determined by a distance from a point to a line test are added to the resection element list. The tumor surface and cylinder surfaces combined define the resection cavity which is specified to be stress-free and at atmospheric pressure.

As the mesh is rotated for each orientation in a condition set, an automatic boundary condition generator [7] classifies the nodes on the brain surface as fixed, allowed to slip along tangent-to-the brain surface, or stress-free according to the varying orientation. Two modifications were made to the generator by V.K. Narendira Kumar et al [7, 17] First, as a consequence of manual optimization of a model to the clinical data, the mean height of those brain surface nodes whose dot products with the gravity vector lay between -0.2 and -0.4 was used as the stress-free level as a better shift recovery[7] resulted. Second, the cerebrospinal fluid (CSF) drainage level is specified such that in each orientation one third of the volume of the brain is submerged as determined by summing the volumes of the submerged elements. Maintaining this fraction across orientations also results in keeping the change in tissue buoyancy force causing brain sag the same across orientations. Craniotomy region placement on the mesh is established via determining which brain surface boundary elements lay within the perimeter of the pre-resection laser range scan cortical surface area defined as the craniotomy using the approach vector as the line of sight.

The nodes composing the elements in the resection list are decoupled from the biphasic model analogous to the removal of its tissue counterpart. The decoupled nodes lack displacement solutions. This includes the node at the tumor center whose displacement is used as a measure. Reconstruction of the solutions for the resected nodes is therefore required. This reconstruction is achieved by using a linear elastic model after obtaining displacements on every node on the resection cavity surface for the boundary conditions. The only missing displacements in the output of the biphasic model are those on the nodes inside the resection hole on the brain surface. They are obtained from thin-plate spline interpolation using nodes within 1.25cm of the hole perimeter as control points. The linear elastic model output is combined with the biphasic model's output to yield a complete volumetric displacement description of the brain from which the shift measures can be derived. Levels of the bins by providing graphical image of the bins via IOT Php web development platform.



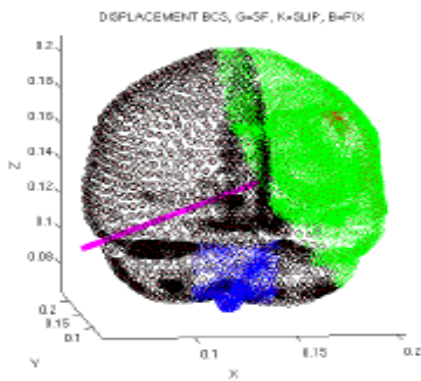
(C)

**Figure 6 :** (A) Representative boundary condition set where green nodes are stress-free (free to deform), black are slip nodes (no movement in the normal direction), blue nodes are fixed, magenta gravity vector indicated. (B) Corresponding CSF drainage level where red are submerged (no drainage) and blue are at atmospheric pressure. (C) Spherical coordinate system for head orientations with neutral gravity  $g = [0 \ 1 \ 0]$  defined to be  $\phi = 0^\circ$ ,  $\theta = 0^\circ$ , i.e.  $[0^\circ \ 0^\circ]$ .

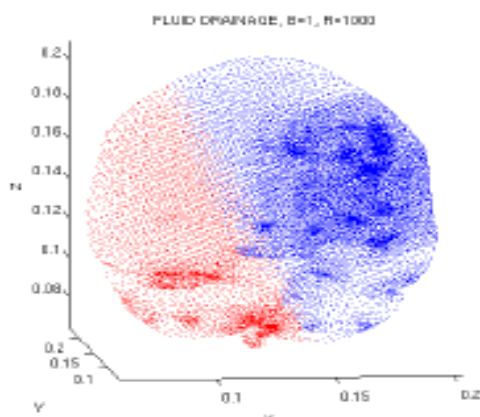
### B. Derived Measures

Using the falx membrane as a support to reduce shift, the neurosurgeon seeks to orient the patient so that gravity-induced shift aids tumor resection. This shift minimization strategy suggested using displacement-based metrics such as lateral shift of the tumor center as viewed along the line of sight established by the 'approach' vector and minimization of change to the field of view in the craniotomy. The tumor center is defined as the node closest to the volumetric centroid of the tumor elements.

The lateral displacement is the perpendicular component of the tumor center's displacement to the 'approach' vector. The change to the field of view was quantified by classifying the brain surface area within the craniotomy using the 'approach' vector as the line of sight. To get a finer resolution of the area contained in the craniotomy, the brain surface is first post-processed by splitting each boundary element into four using extra nodes at the midpoints of each segment to create extra boundary elements. Then the



(A)



(B)

perimeter of the craniotomy in conjunction with the boundary element centroid coordinates is used in a standard point inside a polygon test to segment the brain surface into elements inside and outside the craniotomy.

This segmentation defines an area map. An area map of the boundary elements before deformation is used to delineate the original craniotomy surface. After deformation an area map recording those boundary elements within the craniotomy perimeter is again created. Boundary elements common to both maps are classified as area staying visually the same. Boundary elements visible in the pre-deformation map but not in the post-deformation map are classified as area leaving the craniotomy. Boundary elements visible in the post- map but not in the pre-map become area entering the craniotomy.

**C. Objective function and optimization**

An objective function in the context of least squares minimization is used to evaluate a range of orientations of the patient. Minimization of the lateral displacement would result in the desirable behavior of the tumor center remaining directly beneath the specified point by the surgeon. Minimization of the area leaving the craniotomy promotes maintaining the surgical field of view and proportionately indicates a favorable reduction in surface shift.

**D. Material properties**

**Table 1:** Material properties used in the model

Symbol	Value	Units
$E_{\text{white and gray}}$	2100	N/m <sup>2</sup>
N	0.45	unitless
$\rho_t$	1000	kg/m <sup>3</sup>
$\rho_f$	1000	kg/m <sup>3</sup>
g	9.81	m/s <sup>2</sup>
$\alpha$	1	unitless
1/S	0	unitless
$K_{\text{white}}$	$1 \times 10^{-10}$	m <sup>3</sup> s/kg
$K_{\text{gray}}$	$5 \times 10^{-12}$	m <sup>3</sup> s/kg
$K_c, \text{ white and gray}$	$5.50 \times 10^{-9}$	Pa/s

The material properties for the model in Table 1 conform to those used by Dumpuri et al.[7] with the alteration of the kc value for gray and white matter being made the same value.

**V. EXPERIMENTAL RESULTS**

A clinical case involving a large frontal lobe tumor in the left hemisphere was analyzed. The three orthoviews in Figure 7 show the details of the location and shape of the patient specific falx, the location and extent of the craniotomy used, and the size and position of the tumor within the brain. Involving much of the volume of the left frontal lobe, the tumor had a volume of 63.61 cm<sup>3</sup> and an average radius of 2.48 cm. In Figure 8 the homologous points on the pre LRS and post LRS surfaces are identified.

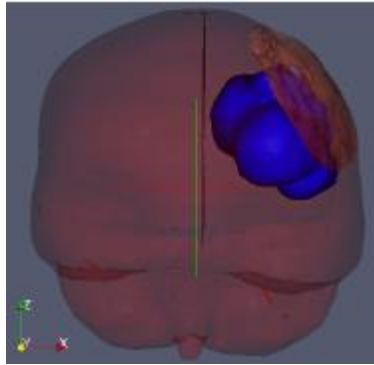
The distribution of the points around the edges of the craniotomy, surrounding the resection hole, and close to the hole’s edge was chosen to provide a good selection of control points for warping the pre LRS surface to the post. The overlay is seen in Figure 8C. Good vessel correspondence especially around the edges of the deformed pre LRS surface on the post surface was observed. The displacements of the homologous points resulting from the surgeon’s chosen orientation for the case were established and the best fit of a model sought. Manual optimization of the model parameters yielded a match of the model’s displacements to those resulting from the surgical orientation with a shift recovery [7] of 67.90% which was in the range of the 70% to 80% reported in the literature. With the model parameters for producing the best match to the data established, an atlas of orientations was created wherein the model combined the effects of both gravity and mannitol.

For the atlas creation a spherical coordinate system for specifying orientations was used. The origin was defined to be the orientation where the default gravity vector lay along the axis from the frontal to

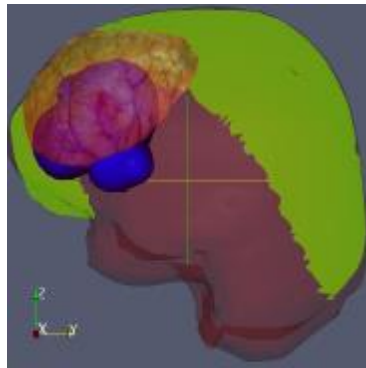
the occipital lobe (the +y axis in Cartesian coordinates) with spherical rotation angles phi and theta of  $[0^\circ 0^\circ]$ .

This orientation corresponded to the patient lay supine. The atlas consisted of 504 orientations with the head being rotated in phi every 6 degrees from -

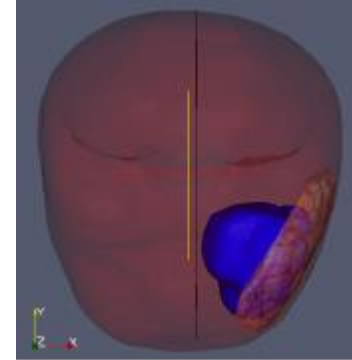
$16^\circ$  to  $146^\circ$  and tilted in theta every 8 degrees from  $-56^\circ$  to  $80^\circ$ . This range of orientations was chosen to guarantee finding the minimal value of the objective function.



(A) Coronal View

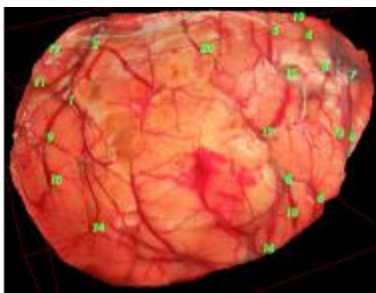


(B) Sagittal View

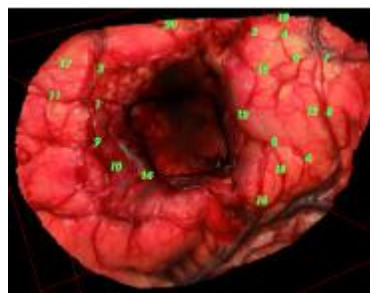


(C) Transverse View

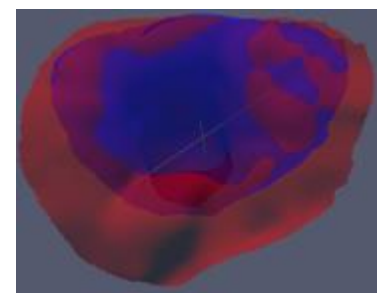
**Figure 7:** Three views of clinical case tumor presentation where brain surface is red, falx is green, tumor is blue, and the craniotomy from a LRS scan is indicated.



(A)

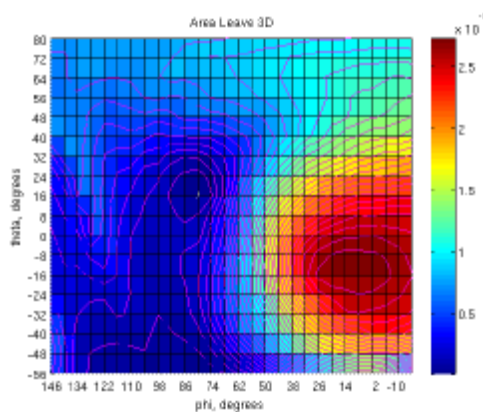


(B)

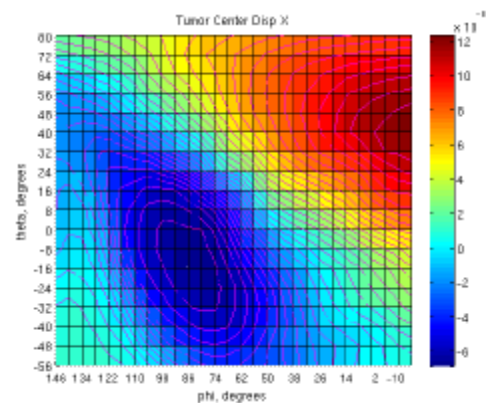


(C)

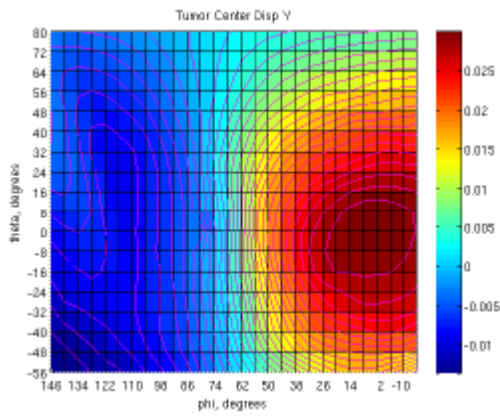
**Figure 8:** (A) 21 points selected on the pre- LRS surface (B) 21 homologous points on the post- LRS surface (C) the pre- LRS surface (blue) warped via a thin-plate spline transformation using the 21 control points to the post- LRS surface (red).



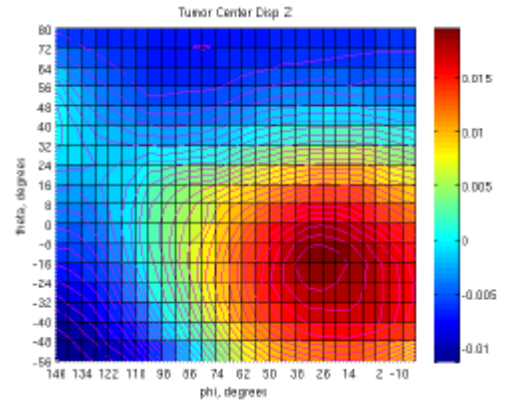
(A) Area leaving craniotomy area [cm<sup>2</sup>]



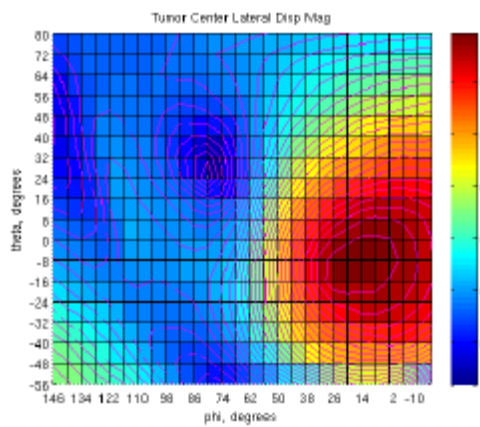
(B) Tumor center lateral displacement x-component [m]



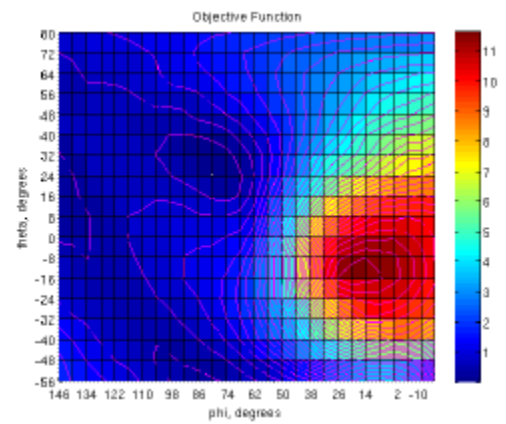
(C) Tumor center lateral displacement y- component [m]



(D) Tumor center lateral displacement z- component [m]

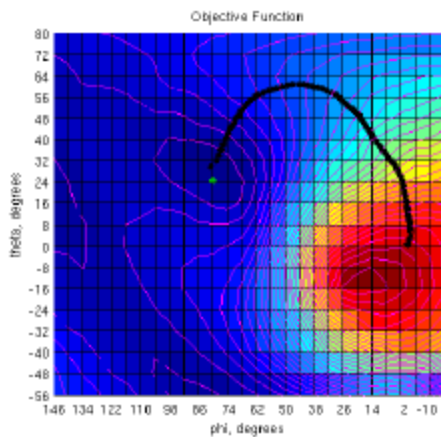


(E) Tumor Center Lateral Displacement Magnitude [m]

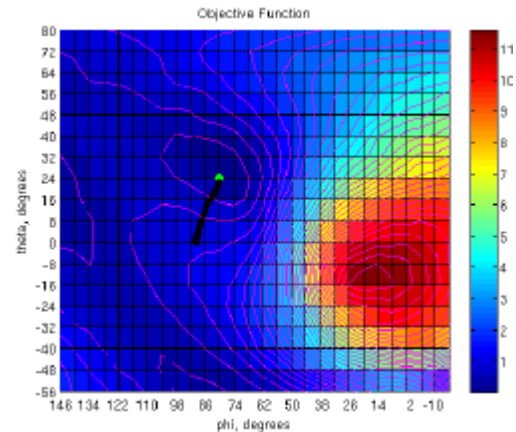


(F) Objective Function

**Figure 9:** Plots of measures over range of orientations and objective function.



(A) Supine Orientation [0° 0°]



(B) Lateral Decubitus Orientation [90° 0°].

**Figure 10:** Optimization pathways shown on the objective function from two initial positions. Black dots are previous orientations and the green dot marks the final orientation.

**Table 2 :** Optimal orientations with spherical rotation angles specified

Orientation	Final Phi	Final Theta
Supine	79.92° 24.36°	24.36°
Lateral Decubitus	79.99°	24.01°
Best Atlas Result	80.00°	24.00°
Best Shift Recovery	66.30°	-7.01°

Figure 9 represents the calculation of the measures over the atlas of orientations. Area leaving the craniotomy was within the range [0, 2.724] cm<sup>2</sup>. The tumor center lateral displacement x- component ranged [-6.86, 12.29] mm, the y displacement [-13.58, 29.94] mm, and the z- displacement [-11.28, 19.54] mm. The magnitude of the lateral displacement was within [0.99,34.53] mm. Orientations where phi > 104° or theta < -16° amounted to over-rotation of the head such that the craniotomy region left the stress-free zone in the boundary condition set and hence were invalid. Discounting of these invalid orientations did not alter the orientation reported as being optimal as determined by the modeling.

Figure 10 presents the optimization path follow by the LM method. Two initial starting poses were used to examine the convergence to the final position, the supine position [0° 0°] and the lateral decubitus [90° 0°] with the tumor Contra lateral to the patient bed. The black markers indicate the sequence of orientations followed down the gradient with the optimal orientation achieved shown as a green marker. In Table 2 the best atlas result is the orientation with the minimum value of the objective function in the atlas. The best shift recovery orientation was the orientation where the model displacements on the nodes corresponding to the 21 LRS surface displacements achieved the highest value of shift recovery for the surgical orientation. The final

orientation angles as reported by the LM method from the two poses are also recorded in Table 2.

**Table 3:** Results for the measures for the four orientations

Measure	Units	LRS	Best Shift	Supine	Model Optimized
Area Enter	cm <sup>2</sup>	17.29	17.07	15.61	8.45
Area Leave	cm <sup>2</sup>	0.13	1.70	25.51	0.41
Area Same	cm <sup>2</sup>	42.14	42.00	18.19	43.29
Craniotomy	cm <sup>2</sup>	42.27	43.70	43.70	43.70
Lateral Shift	mm	N/A	8.45	33.49	0.99

Figure 11 and Table 3 display for visual and quantitative comparison the results of the optimization process seen in Figure 10. Figure 11A shows the area distribution according to the classification of the pre/post overlay of the clinical data. In Figure 11B-D the location of the tumor center before deformation within the craniotomy is shown by the magenta marker and its location after deformation by the green marker. Table 3 records the magnitude of the lateral shift of the tumor center as seen in Figure 11 and the area quantities. The orientation for the supine position in Figure 11C in phi and theta is the default: [0°, 0°]. The orientation in Figure 11B for best shift recovery is at [66.30°, -7.01°]. The orientation in Figure 11D for the model optimization has the angles [80°, 24°].

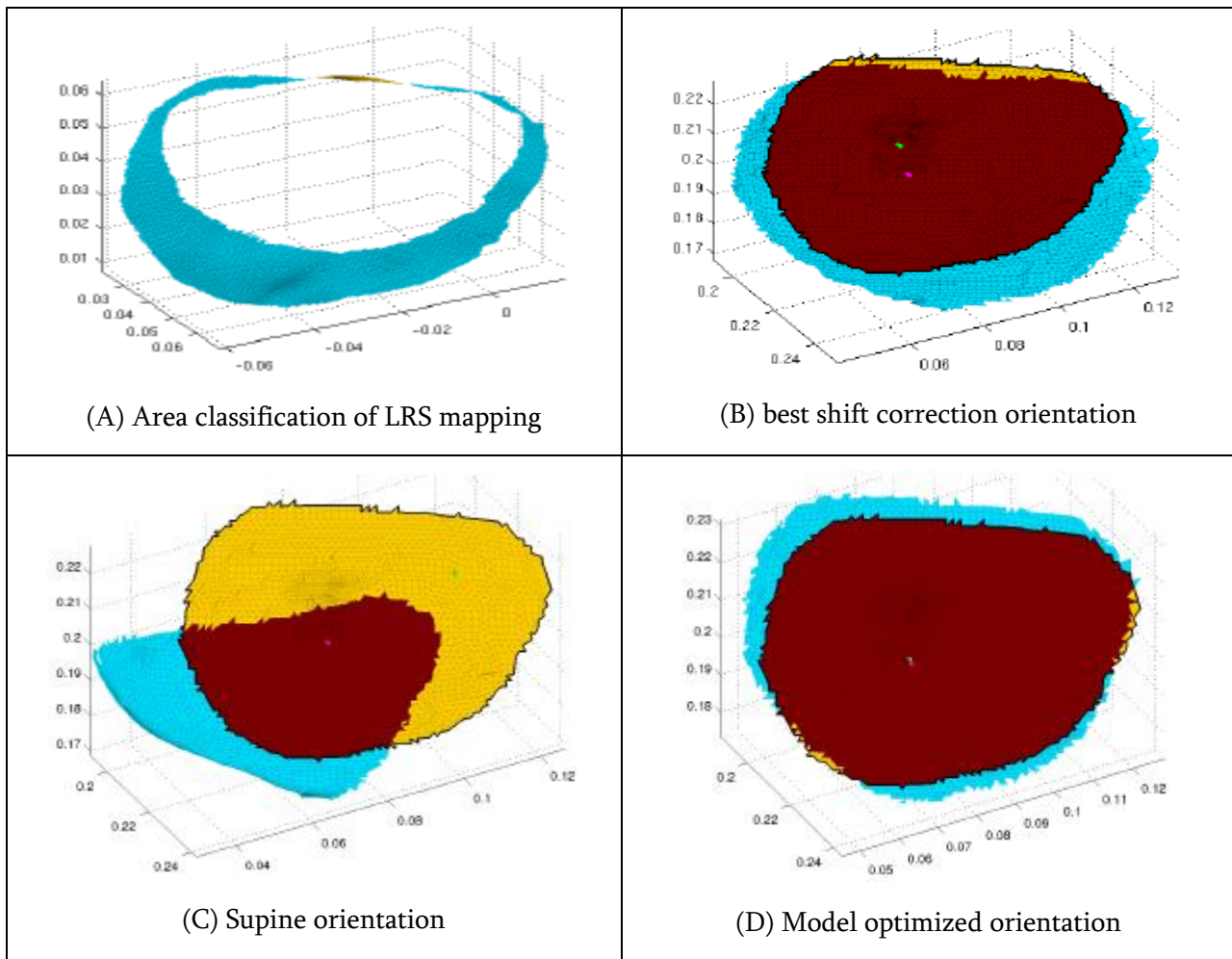


**Figure 11:** Blue boundary elements represent area entering, yellow leaving and red those that remain the same for the craniotomy. The magenta marker is the tumor center projected to the view plane of the craniotomy, and the green the displaced tumor center.

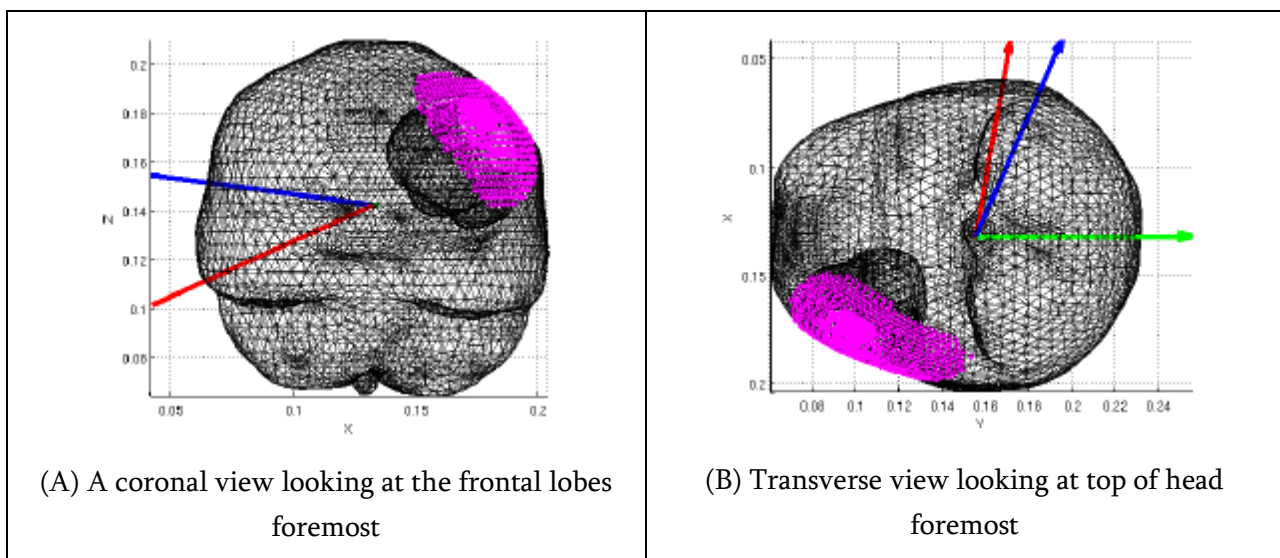


**Figure 12:** Comparison of best shift recovery orientation, optimized model orientation, and supine orientation sag vectors. Magenta region indicates the craniotomy, green is the supine sag vector, blue the shift recovery vector, and red the optimized model vector.

Figure 12 illustrates the differences in applied gravity vectors in the direction of which the brain sags for the standard supine, the best shift recovery match, and the model optimized orientations. Both the best shift recovery orientation and the optimized model orientation result in the craniotomy laying entirely within the stress-free region in the boundary condition set.

## VI. DISCUSSION

Comparison of Figure 11A and 11B, or the fit of the model to the LRS data for the surgical orientation, shows a reasonable correspondence of areal distribution for a shift recovery of 67.90%. Better correspondence of the displacements—i.e. higher shift recovery— would result in area maps more closely approximating that seen in the clinical data and methods of achieving this improvement should be investigated. The area leaving amounts to 0.3% of the craniotomy area for the LRS data and 3.9% for the best shift recovery orientation and it occurs in the same region of the craniotomy for the shift recovery orientation as in the LRS mapping. The areas remaining the same within the craniotomy and entering the craniotomy agree well per Table 3, and the absolute error of the area leaving is small. As can be seen visually in Figure 10 and in the tabulation in Table 2, the optimization converges to an orientation very close to the global optimum. This orientation is successfully achieved from two initial poses, the supine position which is standard for frontal lobe tumors and from the lateral decubitus position. One should note, however, the susceptibility of the LM method to finding local minima, although in this clinical case the atlas global minimum was successfully found. The angular resolution of the atlas is fairly coarse which results in smoothing of the data. This smoothing may have contributed to the successful usage of the LM method by eliminating local minima in which the optimization process might have prematurely terminated.

Previous experiences in the OR have shown that in tumor resection cases where it is desirable to minimize shift the patient is placed by the surgeon in a lateral decubitus position on the side contralateral to the tumor. This position is shown to indeed have the advantage of reducing the anterior-posterior shift, as seen in Figure 11C and quantified in Table 3. For a supine position, Figure 11C indicates a significant amount of area shifting posteriorly with the tumor center lateral shift corroborating this directional shift, whereas Figure 11B indicates the surgeon's attempt to reduce this shift via a lateral decubitus position. A further advantage of the lateral decubitus position is that it makes use of the characteristics of the falx, which acts as a natural constraint on inter-hemispheric movement. In Figure 11B the area distribution and tumor center lateral shift direction suggest that rotation of the head was suitable but an insufficient degree of tilt for shift minimization- the head was tilted in the direction opposite that needed for minimization. However, examination of the shift recovery sag vector in Figure 7 with respect to the placement of the craniotomy and in consideration of how the surgeon sits for surgery suggests that the tilt angle was chosen to permit easier access rather than for shift minimization.

The model optimized result in Figure 11D demonstrates three salient features of interest. First, especially with regards to the supine position yet also regarding the best shift orientation, a marked reduction in lateral shift of the tumor center can be seen. It is anticipated that the possibility of having the tumor stay under the point marked by the surgeon would be a considerable advantage when using image guidance that is not shift compensated. Second, examination of the perimeters of the area entering and leaving and of the craniotomy shows an intriguing degree of concentricity—i.e. the area distributions demonstrate a noticeable degree of symmetry. This concentricity likely corresponds to minimal lateral shift, but more cases would need to be analyzed to prove this conjecture. Third, a significant reduction in the area entering, a factor of a half

compared to supine, means a lesser amount of healthy brain tissue falls into the resection cavity. In combination with the reduction in lateral shift of the tumor center, the reduced amount of area, distributed with the observed concentricity as a thin, fairly uniform band around the edges of the craniotomy, indicates a reduction of movement into the craniotomy of healthy tissue and hence a reduced potential need for retraction.

## VII. CONCLUSION

First realization of an evaluative tool for surgical planning that attempts to optimize surgical approach by means of shift minimization. Currently shift minimization decisions depend mostly on the surgeon's expertise. The evaluative tool described here derives quantitative measures from a biomechanical model that accounts for gravitational forces and the effects of mannitol that can be used in a predictive sense to find an optimal orientation that minimizes brain shift. For a frontal lobe tumor, putting the patient in a lateral decubitus position on the side contralateral to the tumor has clear advantages over the supine position for reducing unfavorable brain shift and potentially reducing retractor usage. While preliminary in nature, this tool demonstrates an interesting clinical potential for aiding surgeons in orientating the patient.

## VIII. REFERENCES

- [1] T. Hartkens, D. L. G. Hill, A. D. Castellano-Smith, D. J. Hawkes, C. R. Maurer, A. J. Martin, W. A. Hall, H. Liu, and C. L. Truwit. Measurement and analysis of brain deformation during neurosurgery. *IEEE Transactions on Medical Imaging*, 22(1):82–92, January 2003.
- [2] C. Nimsky, O. Ganslandt, S. Cerny, P. Hastreiter, G. Greiner, and R. Fahlbusch. Quantification of, visualization of, and compensation for brain shift using intraoperative magnetic resonance imaging. *Neurosurgery*, 47(5):1070–1079, 2000.
- [3] A. Nabavi, P. M. Black, D. T. Gering, C. F. Westin, V. Mehta, R. S. Pergolizzi, M. Ferrant, S. K. Warfield, N. Hata, R. B. Schwartz, W. M. Wells, R. Kikinis, and F. A. Jolesz. Serial intraoperative magnetic resonance imaging of brain shift. *Neurosurgery*, 48(4):787–797, 2001.
- [4] D. W. Roberts, A. Hartov, F. E. Kennedy, M. I. Miga, and K. D. Paulsen. Intraoperative brain shift and deformation: A quantitative analysis of cortical displacement in 28 cases. *Neurosurgery*, 43(4):749–758, 1998.
- [5] K. Ha, P. Dumpuri, M. I. Miga, R. C. Thompson, “Modeling surgical procedures to assist in understanding surgical approach”, *Medical Imaging 2007: Visualization and Image-Guided Procedures: Proc. of the SPIE*, (in press), 2007
- [6] P. Dumpuri, R. C. Thompson, A. Cao, S. Ding, I. Garg, B. M. Dawant, and M. I. Miga, “A fast efficient method to compensate for brain shift for tumor resection therapies measured between preoperative and postoperative tomograms”, *IEEE Transactions on Biomedical Engineering*, (in press), 2009
- [7] P. Dumpuri, R. C. Thompson, B. M. Dawant, A. Cao, M. I. Miga, “An atlas-based method to compensate for brain shift: Preliminary results”, *Medical Image Analysis*, Vol. 11, No. 2., pp.128–145, 2007
- [8] M.A. Biot. “General theory of three-dimensional consolidation”. *J.Appl.Phys.*, 12:155–164, Feb 1941.
- [9] M. I. Miga, K. D. Paulsen, J. M. Lemery, S. D. Eisner, A. Hartov, F. E. Kennedy, and D. W. Roberts. “Model updated image guidance: Initial clinical experiences with gravity-induced brain deformation”. *IEEE Transactions on Medical Imaging*, 18(10):866–874, 1999.
- [10] M. I. Miga, D. W. Roberts, A. Hartov, S. Eisner, J. Lemery, F. E. Kennedy, and K. D. Paulsen. “Updated neuro imaging using intra operative brain modeling and sparse data”. *Stereotactic and Functional Neurosurgery*, 72(2- 4):103–106, 1999.

- [11] M. I. Miga, K. D. Paulsen, P. J. Hoopes, F. E. Kennedy, A. Hartov, and D. W. Roberts. "In vivo quantification of a homogeneous brain deformation model for updating preoperative images during surgery". *IEEE Transactions on Biomedical Engineering*, 47(2):266–273, 2000.
- [12] M. I. Miga, D. W. Roberts, F. E. Kennedy, L. A. Platenik, A. Hartov, K. E. Lunn, and K. D. Paulsen. "Modeling of retraction and resection for intra operative updating of images. *Neurosurgery*", 49(1):75–84, 2001.
- [13] Nagashima T, Shirakuni T, Rapoport S: "A two-dimensional, finite element analysis of vasogenic brain edema," *Neurol Med Chir* 30:1-9, 1990
- [14] M. I. Miga. "Development and quantification of a 3D brain deformation model for model-updated image-guided stereotactic neurosurgery". PhD thesis, Thayer school of Engineering, Dartmouth College, September 1998.
- [15] K.D. Paulsen, M.I. Miga, F.E. Kennedy, P.J. Hoopes, A. Hartov, and D.W. Roberts. "A computational model for tracking subsurface tissue deformation during stereotactic neurosurgery". *IEEE Trans. Biomed. Eng*, 46(2):213–225, Feb 1999.
- [16] M. I. Miga, K. D. Paulsen, F. E. Kennedy, P. J. Hoopes, A. Hartov, and D. W. Roberts. "Initial in-vivo analysis of 3D heterogeneous brain computations for model-updated image-guided Neurosurgery". *Medical Image Computing and Computer-Assisted Intervention 1998: Lecture Notes in Computer Science*, Springer Verlag, New York, 1496, pp.743- 752, 1998.
- [17] V.K. Narendira Kumar et al, "MRI of the Brain in Moving Subjects Application to Fetal, Neonatal and Adult Brain", *International Journal of Information Technology and Computer Science*, ISSN No. 2074-9007 (print), ISSN No. 2074-9015 (online), Page No. 44-50, Vol.: 4, No.: 10, September -2012.
- [18] V.K. Narendira Kumar et al, "3D Brain Tumors and Internal Brain Structures Segmentation in MR Images", *International Journal of Image, Graphics and Signal Processing*, ISSN No. 2074-9074 (print), ISSN No. 2074-9082 (online), Page No. 35-43, Vol.: 4, No.: 1, February - 2012.
- [19] V.K. Narendira Kumar et al, "Segmentation of Striatum Brain Structures from High Resolution Pet Images", *International Journal of Computational Intelligence Research*, ISSN No. 0973-1873 (print), Page No. 51-62, Vol.: 7, No.: 1, 2011.

**Cite this article as :** Dr. V. K. Narendira Kumar, G. Prabhu, N. Geetha, R. Santhosh, "Performance of Assessment Tool for Preoperative Planning of Brain Tumor Resection", *International Journal of Scientific Research in Science, Engineering and Technology (IJSRSET)*, ISSN : 2456-3307, Volume 6 Issue 1, pp. 150-164, January-February 2019. Available at doi : <https://doi.org/10.32628/IJSRSET196134>  
Journal URL : <http://ijsrset.com/IJSRSET196134>